Mathematical Model of Viral Kinetics In Vitro Estimates the Number of E2-CD81 Complexes Necessary for Hepatitis C Virus Entry

Pranesh Padmanabhan[1], **Narendra M. Dixit**[1,2]*

1 Department of Chemical Engineering, Indian Institute of Science, Bangalore, India, **2** Bioinformatics Centre, Indian Institute of Science, Bangalore, India

Abstract

Interaction between the hepatitis C virus (HCV) envelope protein E2 and the host receptor CD81 is essential for HCV entry into target cells. The number of E2-CD81 complexes necessary for HCV entry has remained difficult to estimate experimentally. Using the recently developed cell culture systems that allow persistent HCV infection in vitro, the dependence of HCV entry and kinetics on CD81 expression has been measured. We reasoned that analysis of the latter experiments using a mathematical model of viral kinetics may yield estimates of the number of E2-CD81 complexes necessary for HCV entry. Here, we constructed a mathematical model of HCV viral kinetics in vitro, in which we accounted explicitly for the dependence of HCV entry on CD81 expression. Model predictions of viral kinetics are in quantitative agreement with experimental observations. Specifically, our model predicts triphasic viral kinetics in vitro, where the first phase is characterized by cell proliferation, the second by the infection of susceptible cells and the third by the growth of cells refractory to infection. By fitting model predictions to the above data, we were able to estimate the threshold number of E2-CD81 complexes necessary for HCV entry into human hepatoma-derived cells. We found that depending on the E2-CD81 binding affinity, between 1 and 13 E2-CD81 complexes are necessary for HCV entry. With this estimate, our model captured data from independent experiments that employed different HCV clones and cells with distinct CD81 expression levels, indicating that the estimate is robust. Our study thus quantifies the molecular requirements of HCV entry and suggests guidelines for intervention strategies that target the E2-CD81 interaction. Further, our model presents a framework for quantitative analyses of cell culture studies now extensively employed to investigate HCV infection.

Citation: Padmanabhan P, Dixit NM (2011) Mathematical Model of Viral Kinetics In Vitro Estimates the Number of E2-CD81 Complexes Necessary for Hepatitis C Virus Entry. PLoS Comput Biol 7(12): e1002307. doi:10.1371/journal.pcbi.1002307

Editor: Roland Robert Regoes, ETH, Switzerland

Received July 16, 2011; **Accepted** October 31, 2011; **Published** December 8, 2011

Funding: This work was supported by the Department of Biotechnology Centre of Excellence for Research on Hepatitis C Virus, India. The funders had no role in study design, data collection and analysis, decision to publish, or preparation of the manuscript.

Competing Interests: The authors have declared that no competing interests exist.

* E-mail: narendra@chemeng.iisc.ernet.in

Introduction

HCV entry into target cells is a complex process involving the interactions of the viral envelope proteins E1 and E2 and several cell surface receptors, namely, scavenger receptor class B type I (SR-BI) [1], the tetraspanin CD81 [2,3], and the tight junction proteins claudin-1 (CLDN1) [4] and occludin [5]. Several recent studies suggest a central role for CD81 in HCV entry: E2 has been shown to interact directly with SR-BI and CD81 following viral attachment to a target cell [1,2]. Patient derived neutralizing antibodies appear to target the CD81 binding domains on E2 [6]. Indeed, anti-CD81 antibodies were able to block infection in vitro [3] and in a mouse model [7]. Graft reinfection following liver transplantation was observed recently to select for HCV strains capable of more efficient entry, achieved partly through mutations in the CD81 binding domains on E2 [8]. Expression of human CD81 and occludin was essential for infection of genetically humanized mice [7]. Besides, CLDN1 appears to mediate HCV entry through its association with CD81 [9,10]. Consequently, the E2-CD81 interaction presents a potent target for intervention; drugs that block the E2-CD81 interaction are currently under development [11,12].

How many E2-CD81 complexes must be formed between a virion and a target cell to enable HCV entry? Knowledge of this threshold would determine the number of E2-CD81 complexes that a drug or a vaccine must prevent from forming in order to block viral entry, thus presenting a quantitative guideline for intervention strategies targeting the E2-CD81 interaction. This threshold is currently unknown. Direct observation of the number of E2-CD81 complexes formed before HCV entry has not been possible. Recent cell culture studies have determined the dependence of viral entry and kinetics in vitro on the CD81 expression level on target cells [10,13–18]. In particular, cells expressing higher levels of CD81 were found to be more susceptible to infection [13]. Further, the frequency of cells with low CD81 expression typically increased with time following the exposure of cells to HCV [14,15]. We reasoned that analysis of these observations using a mathematical model of viral kinetics, akin to studies of HIV entry (for example, see [19,20]), may allow estimation of the threshold number of E2-CD81 complexes necessary for HCV entry. While models of HCV viral kinetics in vivo have been employed successfully to analyse patient data and elucidate guidelines for treatment [21–31], models of HCV viral kinetics in vitro have just begun to be formulated.

Author Summary

The interaction between the hepatitis C virus (HCV) envelope protein E2 and the host cell surface receptor CD81 is critical for HCV entry into hepatocytes and presents a promising drug and vaccine target. Yet, the number of E2-CD81 complexes that must be formed between a virus and a target cell to enable viral entry remains unknown. Direct observation of the E2-CD81 complexes preceding viral entry has not been possible. We constructed a mathematical model of HCV viral kinetics in vitro and using it to analyze data from recent cell culture studies obtained estimates of the threshold number of E2-CD81 complexes necessary for HCV entry. We found that depending on the E2-CD81 binding affinity, between 1 and 13 complexes are necessary for HCV entry into human hepatoma-derived cells. Our study thus presents new, quantitative insights into the molecular requirements of HCV entry, which may serve as a guideline for intervention strategies targeting the E2-CD81 interaction. Further, our study shows that HCV viral kinetics in vitro can be described using a mathematical model, thus facilitating quantitative analyses of the wealth of data now emanating from cell culture studies of HCV infection.

Here, we constructed a mathematical model of HCV viral kinetics in vitro that mimics cell culture studies of the dependence of viral entry and kinetics on CD81 expression. Model predictions captured data from several independent experiments quantitatively and yielded estimates of the threshold number of E2-CD81 complexes necessary for HCV entry.

Results

Model formulation

We considered in vitro experiments where a population of target cells, T, with a known distribution of the CD81 expression level across cells is exposed to a population of HCVcc (cell culture adapted) virions, V, and the progression of infection followed [13–15]. We modelled the ensuing viral kinetics as follows (Fig. 1). We first considered a single virus-cell pair with the virus attached to the cell by interactions that precede E2-CD81 binding [12]. E2 and CD81 then interact to form E2-CD81 complexes. We computed the mean number of these complexes formed at equilibrium, $\overline{N_C}$, as a function of the CD81 expression level, n_i, on the cell. Assuming that the number of complexes formed, N_C, followed a Poisson distribution with mean $\overline{N_C}$, we computed the probability, S_i, that N_C was larger than a threshold number N_C^T. We assumed that viral entry (and subsequently infection) occurred if $N_C \geq N_C^T$ (Fig. 1A). Thus, S_i yielded the relative susceptibility to infection of a cell with CD81 expression level n_i.

We next considered the population of cells exposed to virions (Fig. 1B). We divided the cells into different subpopulations T_i with distinct CD81 expression levels n_i and hence different susceptibilities S_i, where $i = 1, 2, \ldots, K$. Cells in each subpopulation were assumed to proliferate, die, or be infected at a rate proportional to S_i. The resulting infected cells, I_i, were lost at enhanced rates compared to T_i due to virus-induced cytopathicity in vitro [15,32]. Free virions were produced by infected cells and were cleared. With this description, we constructed dynamical equations to predict the time-evolution of each of the uninfected and infected cell subpopulations and the population of free virions and compared our predictions with experiments (Methods).

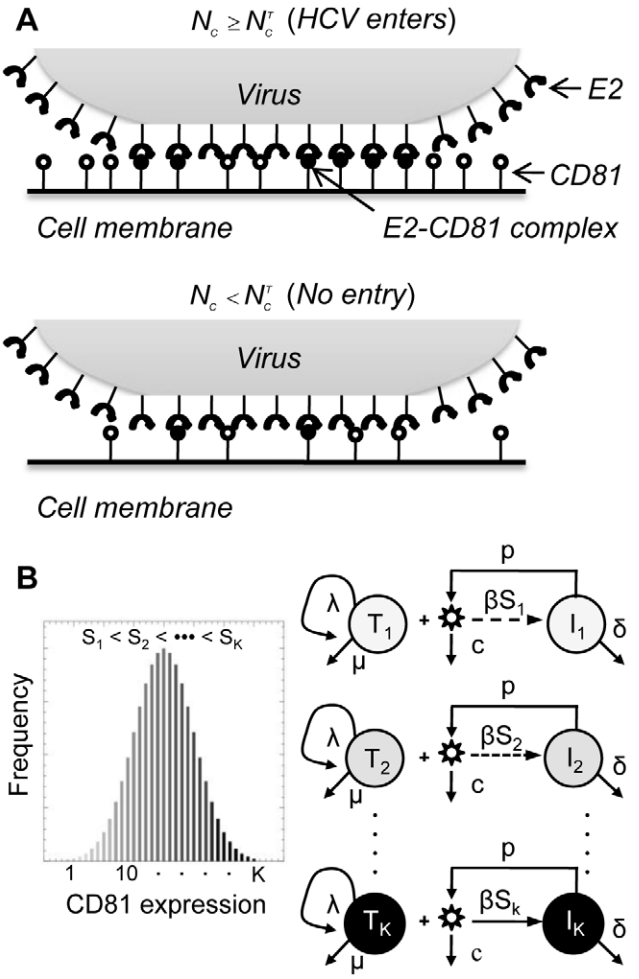

Figure 1. Schematic of the model. (A) HCV enters a target cell if the number of E2-CD81 complexes formed across the virus-cell pair, N_C, exceeds the threshold, N_C^T (top), but not otherwise (bottom). (B) Viral kinetics following the exposure of cells with a distribution of the CD81 expression level (left) to virions in vitro is determined by the time-evolution of subpopulations 1 through K of cells with distinct CD81 expression levels and hence different susceptibilities to HCV entry (right).
doi:10.1371/journal.pcbi.1002307.g001

Model predictions

Triphasic viral kinetics in vitro. When cells with a log-normal distribution of the CD81 expression level (Fig. 2A inset) were exposed to virions in vitro, we found that infection proceeded in three phases (Figs. 2A and B). In the first phase, the population of uninfected cells, T, rose, as their net proliferation rate dominated their loss rate by infection. At the same time, exposure of T to virions resulted in the growth of infected cells, I. Initially, because I was small, viral production was dominated by clearance, resulting in a decline of the viral load, V. As I increased, viral production compensated for clearance and V began to rise. Subsequently, V evolved proportionally to I, indicating the establishment of a pseudo-steady state between viral production and clearance, $pI \approx cV$.

In the second phase, V was sufficiently large that the loss of T by infection outweighed cell proliferation, resulting in a decline of T (Fig. 2A). This decline was consequently associated with a steep rise in I and correspondingly V (Fig. 2B). In the third phase, T rose again while I and V remained nearly constant. This third

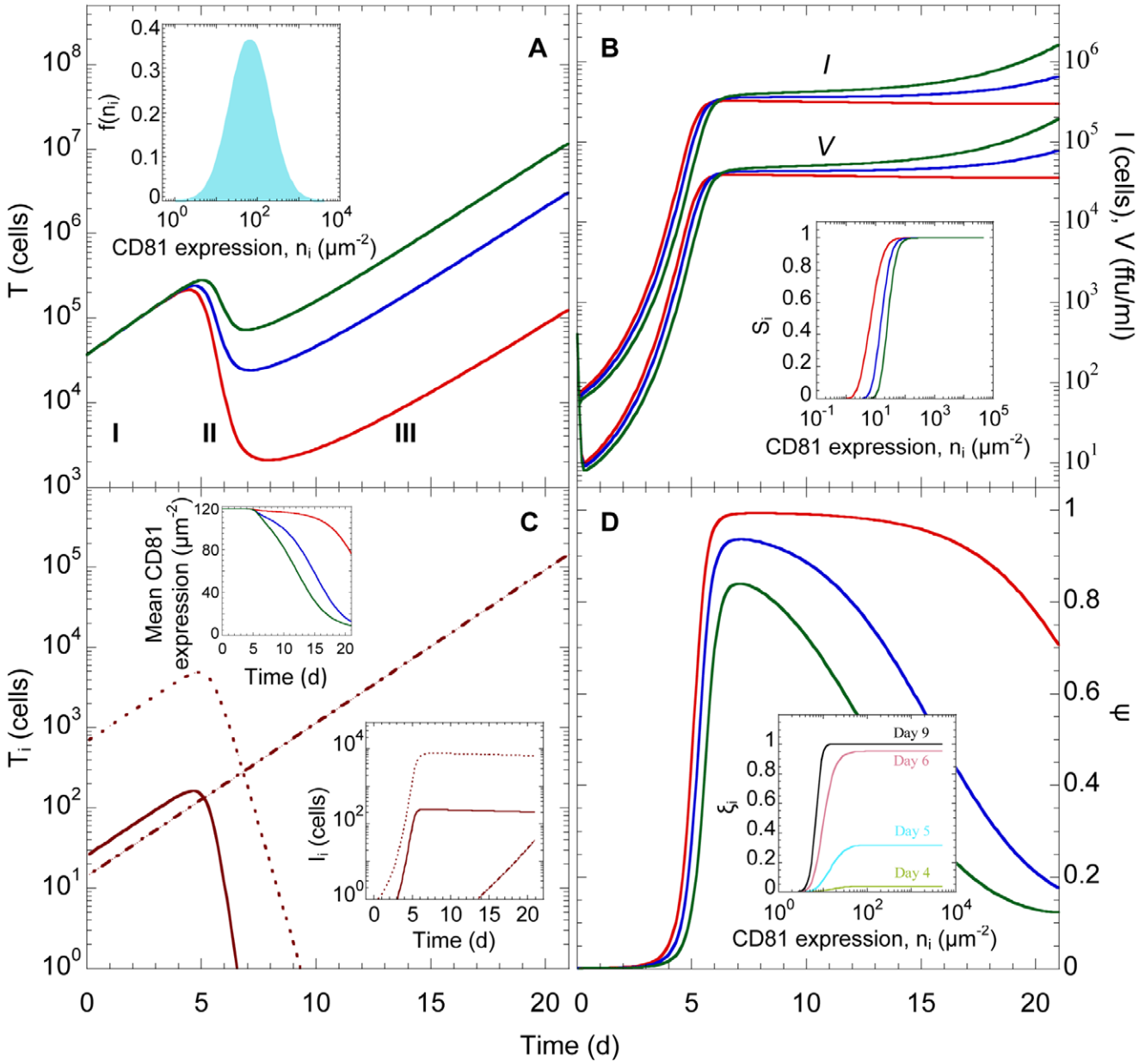

Figure 2. Model predictions of HCV viral kinetics in vitro. The time evolution of (A) uninfected cells, T, (B) infected cells, I, and viral load, V, (C) uninfected cell sub-populations, T_i, and (lower inset) infected cell sub-populations, I_i, corresponding to $S_i \approx 10^{-5}$ (dot-dashed line), 0.5 (dotted line) and 1 (solid line), and (D) the total fraction of cells infected, ψ. The initial CD81 distribution, $f(n_i)$, as a function of the CD81 expression level, n_i, is presented in the inset in (A). The three phases of infection are also marked in (A). Inset in (B) shows S_i as a function of n_i. Upper inset in (C) shows the time evolution of the mean CD81 surface density. Inset in (D) shows the fractions of cells infected in sub-populations with distinct CD81 expression levels, ξ_i, at different post-infection times. In (A), (B), (D) and the upper inset in (C), $N_C^T = 2$ (red line), 4 (blue line), and 6 (green line). In (C) and the inset in (D), $N_C^T = 4$. Other parameter values employed are $\lambda = 0.44\,\mathrm{d}^{-1}$; $\mu = 1.7 \times 10^{-4}\,\mathrm{d}^{-1}$; $\delta = 0.011\,\mathrm{d}^{-1}$; $p = 2.78\,\mathrm{ffu \cdot (ml \cdot d)^{-1}}$; $c = 23.2\,\mathrm{d}^{-1}$; $\beta = 1.2 \times 10^{-4}\,\mathrm{ml \cdot (ffu \cdot d)^{-1}}$; $K_D = 1.7 \times 10^{-4}$ M. Initial conditions are $T(0) = 3.7 \times 10^4$ cells; $I(0) = 0$; $V(0) = 400\,\mathrm{ffu \cdot ml^{-1}}$.
doi:10.1371/journal.pcbi.1002307.g002

phase resulted from diverse kinetic profiles of subpopulations of cells, T_i, expressing different levels of CD81, which we describe below.

Dependence of viral kinetics on CD81 expression. The relative susceptibility of cells to infection, S_i, depends on the CD81 expression level, n_i, and the parameters N_C^T and K_D (equilibrium dissociation constant or the inverse of affinity) (Eqs. (4) and (5)). For fixed N_C^T and K_D, S_i increased with n_i (Fig. 2B inset). Above a certain n_i ($\approx 10^2\,\mu\mathrm{m}^{-2}$), CD81 did not limit entry and cells were nearly completely susceptible to infection ($S_i \approx 1$). At the same time, below a certain n_i ($\approx 1\,\mu\mathrm{m}^{-2}$), cells were refractory to infection ($S_i \approx 0$). This variation in S_i led to diverse kinetic profiles.

In the first phase of viral kinetics, all subpopulations T_i grew because infection rates were low and cell proliferation dominated (Fig. 2C). In the second phase, T_i declined for subpopulations with sufficiently large S_i that infection dominated proliferation (e.g., $S_i \approx 0.5$ and ≈ 1 in Fig. 2C). The corresponding I_i accordingly rose (Fig. 2C lower inset). Eventually, nearly all cells in these subpopulations were infected and T_i vanished leaving behind a pool of infected cells. This pool remained constant over the ≈ 20 d

period considered here because the lifespan of infected cells assumed was much larger, ≈ 100 d. Correspondingly, V also remained nearly constant (Fig. 2B). In contrast, subpopulations with low S_i were not easily infected and continued to grow throughout (*e.g.*, $S_i \approx 10^{-5}$ in Fig. 2C). The growth of the latter cells resulted in the rise of T in the third phase of infection (Fig. 2A).

Indeed, at any time $t>0$, the fraction of cells infected within any subpopulation, ξ_i, increased with n_i (Fig. 2D inset). For large n_i, CD81 did not limit infection ($S_i \approx 1$) so that ξ_i evolved independently of n_i. Eventually, all cells in the latter subpopulations were infected and ξ_i approached 1. Below a certain n_i, however, S_i was so low that hardly any cells were infected and ξ_i remained vanishingly small. These latter subpopulations, refractory to infection, ultimately dominated the target cell population. That a majority of the cells in the third phase was refractory to infection was also evident from the time-evolution of the total fraction of cells infected, ψ (Fig. 2D). ψ increased initially as cells with high n_i were infected. After a majority of the latter cells was infected, I remained constant whereas the population of cells refractory to infection increased, resulting in a decrease of ψ. Accordingly, the mean CD81 expression also decreased (Fig. 2C upper inset). Even with low susceptibility, however, stochastic events may result in the formation of the threshold number of complexes and allow viral entry. As T_i increased, the frequency of such stochastic events grew and resulted in the growth of the corresponding I_i (Fig. 2C lower inset), which in turn resulted in the subtle rise of I and V towards the end of the third phase (Fig. 2B).

Influence of model parameters. As N_C^T increased, S_i decreased (Fig. 2B inset), increasing the fraction of cells refractory to infection and hence lowering ψ (Fig. 2D). Accordingly, the rise of T in the third phase was enhanced upon increasing N_C^T (Fig. 2A). As T increased, the frequency of stochastic events leading to entry into cells with low S_i increased and resulted in a slightly greater increase of I and V towards the end of the third phase (Fig. 2B). Variations in other model parameters introduced similar quantitative variations but did not alter the triphasic kinetics qualitatively (Fig. S1). Below, we present comparisons of our model with experiments.

Comparison with experiments

HCV viral kinetics in vitro. We considered first the experiments of Zhong et al. [15], who measured the kinetics of the growth of Huh-7.5.1 cells with and without exposure to JFH-1 virions. We solved model equations using the initial CD81 distribution corresponding to Huh-7.5 cells [13] (Methods) (Fig. S2). We fit model predictions of the time-evolution of the population of viable cells, T_v, and of the ratio of the populations of dead and viable cells, T_d/T_v, simultaneously to the corresponding experimental data in the absence of infection ($V=0$). Our model provided good fits to the data and yielded estimates of the proliferation and death rates, λ and μ, of uninfected Huh-7.5.1 cells (Fig. 3A). It follows from our model that in the absence of infection ($V=0$), $T_v = T_0 \exp((\lambda-\mu)t)$ and $T_d/T_v = \mu(1-1/T_v)/(\lambda-\mu) \approx \mu/(\lambda-\mu)$, where T_0 is the population of cells at the start of infection. In agreement, T_v rose linearly on a semi-log plot and the ratio T_d/T_v remained nearly constant (Fig. 3A).

Using λ and μ estimated thus and recognizing that viral production and clearance rapidly attain pseudo-steady state ($\frac{dV}{dt} \approx 0$, which implies that $V \approx \frac{pI}{c}$), we next fit our predictions of the time-evolution of T_v, the ratio T_d/T_v, and the viral load, V, simultaneously to the corresponding measurements during infection ($V>0$) using δ, β, ω ($=p/c$), and N_C^T as adjustable parameters for different values of K_D. (We employed a truncated Gaussian approximation to the Poisson probability for S_i (Fig. S3).) Model predictions again provided good fits to the data (Fig. 3B and Fig. S4A) indicating the ability of our model to capture experimental observations quantitatively.

The data were consistent with the triphasic viral kinetics predicted by our model. T_v displayed an initial rise followed by a plateau and a subsequent rise (Fig. 3B). V displayed an initial rise and a plateau. The ratio T_d/T_v rose initially, attained a maximum, and then declined. In our model calculations, both T and I rose in the first phase (Fig. 2), in agreement with the initial rise of T_v, which is the sum of T and I, in the experiments. In the second phase, T declined primarily due to infection, giving rise to I, which maintained a nearly constant sum of T and I, consistent with the plateau in T_v. In the third phase, I remained nearly constant or rose marginally, whereas T rose significantly, in agreement with the subsequent rise of T_v. Similarly, the rise of V in the second phase followed by the plateau were also in agreement with the trends predicted (Fig. 2). In the first phase, however, V initially declined and then rose as I increased (Fig. 2). The data considered here were collected from day 2 post-infection (Fig. 3B), by which period pseudo-steady state between viral production and clearance is expected to be established and the initial decline of V is therefore not expected to be observed. Finally, the initial rise of T_d/T_v corresponded to the rise of I in the first and second phases; I had lifespans shorter than T due to virus-induced cytopathicity so that higher values of I resulted in greater T_d. The subsequent drop in T_d/T_v corresponded to the rise of T in the third phase, which increased T_v and also lowered the overall rate of cell death.

Threshold number of E2-CD81 complexes necessary for entry. From the above fits, for each value of K_D in the range $\sim 10^{-5} - 10^{-4}$ M, we obtained a corresponding best-fit estimate of N_C^T (Fig. 4, Table S1). For example, $N_C^T = 9$ (95% CI: 6–13) when $K_D = 1.7 \times 10^{-5}$ M and $N_C^T = 3$ (95% CI: 2–4) when $K_D = 1.7 \times 10^{-4}$ M. The best-fits thus suggested that depending on the affinity of E2 for CD81, between 1 and 13 E2-CD81 complexes across a virus-cell pair were necessary for the entry of JFH-1 virions into Huh-7.5.1 cells.

Robustness of parameter estimates. To test the robustness of our estimate of N_C^T, we applied our model to the analysis of two independent datasets of viral entry and kinetics in vitro. Koutsoudakis et al. [13] exposed an equal mixture of Huh7-Lunet and Lunet/CD81 cells to Jc1 virions at two different MOIs and measured the fractions of cells infected in sub-populations with distinct CD81 expression levels at day 3 post-infection. To compare our model predictions with their data, we employed the initial CD81 distribution obtained by averaging the distributions on Huh7-Lunet and Lunet/CD81 cells (Fig. S2) and predicted the fraction of cells infected in cell sub-populations with distinct CD81 expression levels, ξ_i. We fixed λ, μ, and δ to the values estimated above (Table 1). The two initial MOIs employed would lead to different pseudo-steady states between viral production and clearance; i.e., $V \approx \frac{pI}{c}$ would still hold, but the values of V and I would be different when the pseudo steady state is reached in the two cases. To account explicitly for the different initial MOIs employed, we therefore relaxed the pseudo-steady state approximation in our model. We obtained c, the viral clearance rate, by fitting our model predictions without the pseudo-steady state approximation to the above data of Zhong et al. [15] (Fig. S5). We then fit our predictions of ξ_i to the data of Koutsoudakis et al. [13] with both the initial MOIs simultaneously using the appropriate initial conditions and N_C^T, p and β as adjustable parameters for different values of K_D. In effect, we assumed that

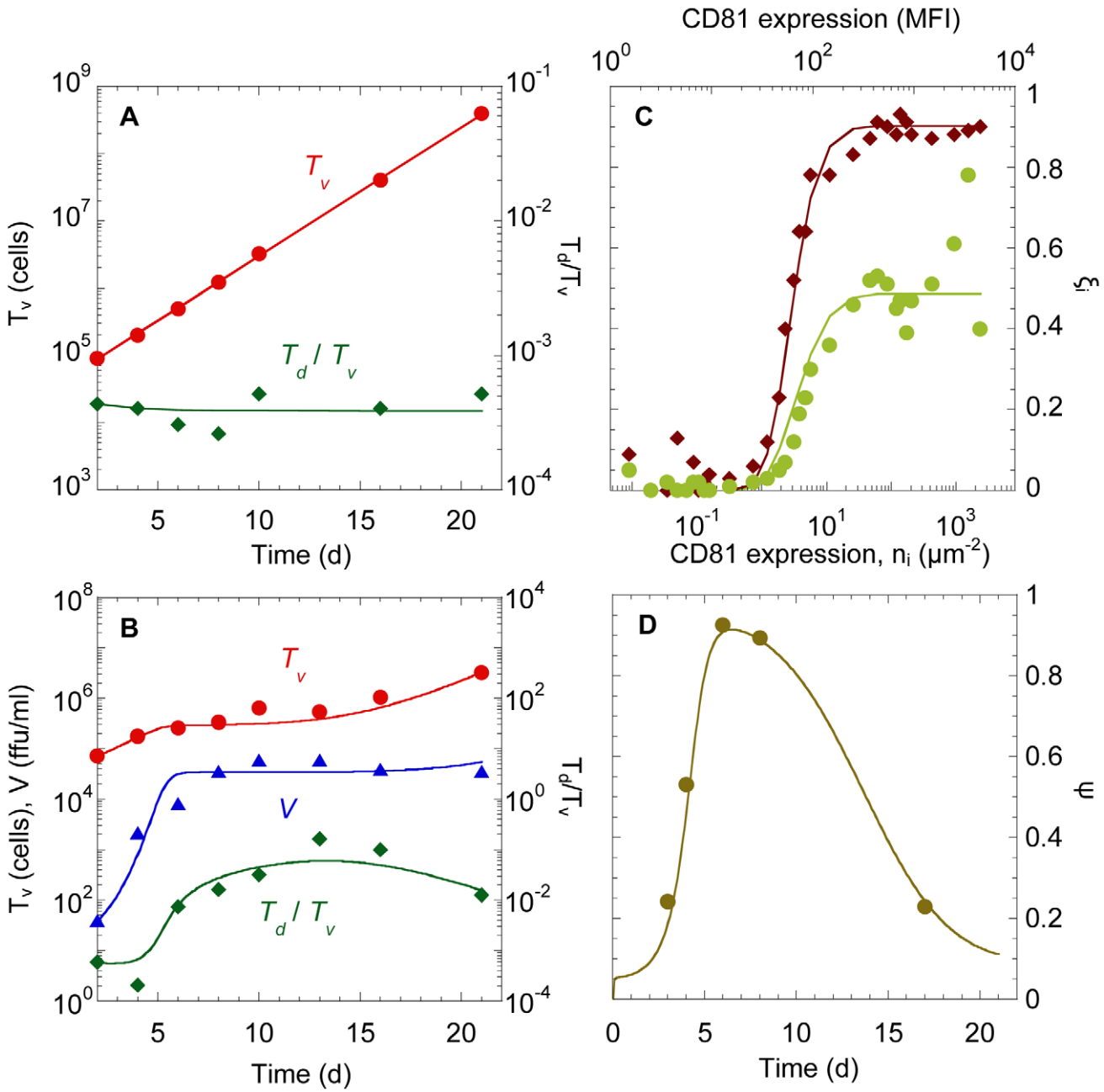

Figure 3. Comparisons with experiments. (A) Fits of model predictions (lines) to data [15] (symbols) of the time-evolution of the population of viable cells, T_v, and the ratio of the populations of dead and viable cells, T_d/T_v, in the absence of infection using λ and μ as adjustable parameters. Initial conditions: $T(2)=9\times10^4$ *cells* and $T_d(2)=40$ *cells*. (B) Fits of model predictions (lines) to data (symbols) [15] of the time-evolution of T_v, T_d/T_v, and the viral titre, V, using δ, β, $\omega(=p/c)$, and N_C^T as adjustable parameters and with $K_D=1.7\times10^{-4}M$. Initial conditions: $V(2)=40\,\mathrm{ffu\cdot ml^{-1}}$; $I(2)=\omega V(2)$; $T(2)=9\times10^4-I(2)$ cells; $T_d(2)=40$ cells. (C) Fits of model predictions (lines) of fractions of cells infected in sub-populations with distinct CD81 expression levels, ξ_i, at day 3 post-infection to data [13] (symbols) using N_C^T, p and β as adjustable parameters and with $K_D=1.7\times10^{-4}$ M. Initial conditions: $T(0)=10^5$ cells; $I(0)=0$; $V(0)=10^5\,\mathrm{TCID_{50}}$ (MOI$\sim$1; circles) or $5\times10^5\,\mathrm{TCID_{50}}$ (MOI$\sim$5; diamonds). Fits with other values of K_D are presented in Fig. S4. The best-fit parameters are in Tables S1 and S2. (D) Model prediction (line) of the time-evolution of the fraction of cells infected, ψ, compared with data [14] (symbols). Initial conditions used: $T(0)=3.7\times10^4$ cells; $V(0)=12000\,\mathrm{ffu\cdot ml^{-1}}$ (MOI$\sim$0.3); $I(0)=0$. Other parameters are the same as in (A). Comparisons with other values of K_D are presented in Fig. S4.
doi:10.1371/journal.pcbi.1002307.g003

the differences in the viral clones, JFH-1 and Jc1, and the cell lines, Huh7.5 and the combination of Huh7-Lunet and Lunet/CD81, affected the viral production rate and/or the infection rate.

Model predictions again provided excellent fits to the data (Fig. 3C and Fig. S4B). For CD81 expression levels $<0.1\,\mu m^{-2}$, ξ_i remained negligible for both MOIs, indicating that these subpopulations were refractory to infection. For higher expression levels, ξ_i increased with CD81 expression and reached a plateau at an expression level of $\sim10^2\,\mu m^{-2}$, beyond which viral entry was not limited by CD81. The plateau attained different values for the two MOIs, as expected from the different underlying viral kinetics. With MOI of 5, $\sim$90% of the cells with excess CD81 were infected

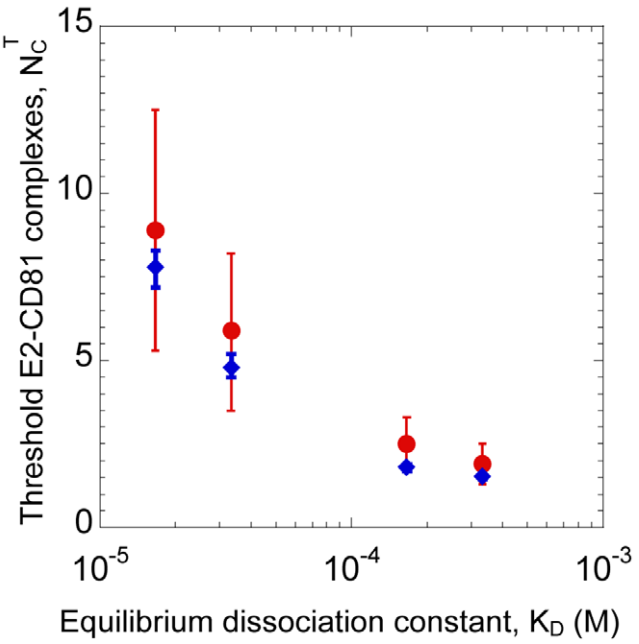

Figure 4. Threshold number of E2-CD81 complexes. Estimates of N_C^T for different values of K_D obtained from fits of model predictions to the data of Zhong et al. [15] (circles) and Koutsoudakis et al. [13] (diamonds) (Fig. S4). Error bars are 95% confidence intervals.
doi:10.1371/journal.pcbi.1002307.g004

by day 3, whereas with MOI of 1, ~50% of the cells with excess CD81 were infected. The resulting estimates of N_C^T were in close agreement with the estimates obtained above (Fig. 4 and Table S2), giving us confidence in our model and our estimates of N_C^T. We note that model predictions of the total percentage of cells infected, ψ, at MOI 5 and 1 (~31% and ~23%, respectively) were lower than the corresponding measurements (57% and 29%). We found that altering the initial mixture (1:4 Huh7-Lunet and Lunet/CD81 cells) or the initial distribution of CD81 expression brought our predictions (~50% and ~30%, respectively) close to the experiments. Fits to the data and the resulting estimates of N_C^T remained unaltered; the only differences were in the estimates of p and β, again indicating the robustness of the estimates of N_C^T.

We considered finally the experiments of Tscherne et al. [14], where the fraction of Huh 7.5 cells infected with J6/JFH virus was measured as a function of time following the onset of infection. We solved our model equations without any adjustable parameters and with the appropriate initial conditions and predicted the time-evolution of the fraction of cells infected, ψ (Fig. 3D). Following the onset of infection, ψ increased and reached a maximum of 90% at day 5 post-infection. Subsequently, cells refractory to infection began to outgrow the susceptible population and ψ decreased, reaching ~20% by day 17 post-infection. Our model captured the measured evolution of ψ quantitatively (Fig. 3D and Fig. S4C). The agreement between model predictions without any adjustable parameters and experimental observations represented a successful validation of our model as well as the parameter estimates obtained above.

Discussion

Analysis of experimental data using mathematical models has provided crucial insights into disease pathogenesis and the effectiveness of drugs and established guidelines for rational optimization of therapy for HCV infection [21–31,33,34]. The recent development of cell culture systems that allow persistent HCV infection in vitro [35–38] has yielded a wealth of new data on HCV replication, evolution, and the impact of drugs. Analysis of this data is expected to provide further insights into HCV pathogenesis and outcomes of therapy, but has been precluded by the lack of mathematical models of HCV viral kinetics in vitro. Indeed, significant efforts are underway to construct models of the intracellular replication and evolution of HCV with the aim of elucidating the activity of direct acting antiviral drugs [39–41]. Here, we have constructed a mathematical model of HCV viral kinetics in vitro. Applying it to the analysis of data from several recent cell culture studies, we obtained quantitative insights into the molecular requirements of HCV entry. We estimated that depending on the binding affinity of E2 and CD81, between 1 and 13 E2-CD81 complexes are necessary for HCVcc entry into human hepatoma-derived cells.

Our estimate provides a quantitative guideline for the optimal usage of drugs and vaccines that target the E2-CD81 interaction: A potent drug or vaccine must ensure that not more than 1–13 E2-CD81 complexes are formed across a virus-cell pair in order to prevent viral entry. This guideline assumes significance as drugs that target the E2-CD81 interaction are under development [11,12] and may become part of future treatments involving direct acting antiviral agents that seek to overcome the limitations of the current interferon-ribavirin-based treatments [42]. Further, a recent analysis of the HCV quasispecies in six patients who

Table 1. Summary of model parameters and their values employed.

Parameter	Description	Value (95% CI)[a]	Source
λ	Proliferation rate of target cells	0.44 (0.43–0.46) d^{-1}	Best-fit (Fig. 3A)
μ	Death rate of target cells	1.7 (1.4–2.0)×10^{-4} d^{-1}	Best-fit (Fig. 3A)
δ	Death rate of infected cells	1.1 (0.4–1.8)×10^{-2} d^{-1}	Best-fit (Fig. 3B)
β	Infection rate of cells with excess CD81 expression	1.2 (0.6–1.8)×10^{-4} ml•(ffu•d)$^{-1}$	Best-fit (Fig. 3B)
ω	Ratio of viral production rate per cell (p) and clearance rate (c)	0.12 (0.06–0.19) ffu•ml^{-1}	Best-fit (Fig. 3B)
c	Clearance rate	23.2 d^{-1}	Best-fit (Fig. S5)
K_D	Equilibrium dissociation constant of the E2-CD81 binding reaction	10^{-4}–10^{-5} M	Varied
n_E	Number density of E2 molecules on HCV	2.3×10^4 μm^{-2}	[53]
A	Virus-cell contact area	1.3×10^{-3} μm^2	[54]

[a]Typical values employed. Variations are indicated in the text and in figure legends.
doi:10.1371/journal.pcbi.1002307.t001

underwent liver transplantation revealed that viral strains capable of more efficient entry, achieved through modulation of the CD81 dependence of viral entry, were selected following liver transplantation [8]. Blocking E2-CD81 interactions effectively, for which our estimate presents a quantitative criterion, may thus be a promising avenue to prevent graft reinfection following liver transplantation.

In an earlier study, Koutsoudakis et al. [13] estimated that a cell must express >70000 CD81 molecules to allow HCV entry. This threshold was identified as follows. In independent experiments, cells with widely varying distributions of CD81 were exposed to HCV at low MOI in culture and the percentage of cells infected at day 5 was measured. This latter percentage was found to correlate well with the percentage of cells initially expressing >70000 CD81 molecules/cell. For instance, with Huh7.5 cells, the percentage of cells infected at day 5 was 91.5 and the percentage expressing >70000 CD81 molecules/cell at day 0 was 93, and with Huh7-Lunet cells, which express fewer CD81 molecules than Huh7.5 cells, the percentages were 11.2 and 17, respectively. Based on this correlation, Koutsoudakis et al. suggested 70000 CD81 molecules/cell as the threshold for entry. Our present analysis suggests that the underlying viral kinetics may render this estimate an upper bound. Virus-induced cytopathicity in culture would result in the loss of susceptible cells and therefore a continuous decrease in the frequency of susceptible cells with time. Consequently, the percentage of cells susceptible initially is expected to be higher than the percentage of cells susceptible–and hence even higher than the percentage infected–at day 5 post-infection. The higher percentage of cells susceptible initially would therefore imply a threshold smaller than 70000 molecules/cell. This is also evident in the experiments of Koutsoudakis et al., where cells with lower CD81 expression (MFI~50) than 70000 molecules/cell (MFI~100) were infected (see Fig. 3C). From our analysis, we identified the threshold number of E2-CD81 complexes and not CD81 molecules necessary for entry. Because stochastic events can result in the formation of the requisite number of complexes, cells expressing few CD81 molecules have small but nonzero susceptibilities to infection. Indeed, we found using parameters employed in Fig. 3D that a small percentage of cells expressing as few as ~10000 CD81 molecules was infected by day 5. More recently, Zhang et al. [18] have argued that a substantially smaller expression level than suggested by Koutsoudakis et al. may suffice for entry and that CD81 may also be necessary, perhaps at higher expression levels, for post-entry events. Our model does not distinguish between entry and post-entry requirements of CD81. Our estimate of 1–13 E2-CD81 complexes defines successful infection of a cell and combines the requirements for entry and any post-entry steps [17,18].

Our model yielded good fits to data with K_D in the range $\sim 10^{-5}-10^{-4}$ M, which is higher than the value, $\sim 10^{-7}$ M, determined using recombinant E2 and soluble CD81 [43]. (Fits with $K_D \sim 10^{-7}$ M were poor (not shown).) This discrepancy may be because the binding affinity when the proteins are in solution may be different from that when the proteins are restricted to membranes [44], recombinant E2 may not accurately mimic the true E2-CD81 interaction [45], and/or only a fraction of the CD81 may lie outside tetraspanin-enriched microdomains and/or be associated with CLDN1 and therefore available for binding E2 [10,46]. The E2-CD81 binding affinity in situ remains to be determined. Our model yielded best-fit values of the threshold number of complexes, N_C^T, that decreased as K_D increased (Fig. 4). For a given CD81 expression level, the mean number of E2-CD81 complexes formed decreased as K_D increased, lowering susceptibility (Eqs. (4) and (5)). Decreasing N_C^T restored this susceptibility (Fig. 2B inset and Fig. S6), thus ensuring that the resulting viral kinetics was conserved and in agreement with data. This does not imply, however, that viral strains with lower E2-CD81 affinity (higher K_D) would require fewer E2-CD81 complexes for entry. On the contrary, given a value of N_C^T, our model predicts that a cell would be less susceptible to entry of viral strains with higher K_D.

Our model was designed to mimic experiments that examined the influence of CD81 expression on viral entry and kinetics [13–15]. In these experiments, cells with high CD81 expression were preferentially infected and lost due to virus-induced cytopathicity, and cells with low CD81 expression, refractory to infection, eventually dominated the culture, suggesting that CD81 expression limited entry. Accordingly, our model assumed that other entry receptors were not limiting. Our model then predicted triphasic viral kinetics in vitro, in agreement with experiments. We note that the origins of the triphasic pattern here are distinct from the triphasic viral load decline in some patients undergoing combination therapy, the latter due to liver homeostatic mechanisms [25]. Further, the triphasic kinetics is a short-term phenomenon (~2–3 weeks). Over longer periods, viral evolution may alter the kinetics substantially [15], which our model does not consider. Nonetheless, our model can be readily adapted to the scenario where a receptor other than CD81 is limiting and may thus serve to quantify the requirements of that receptor for HCV entry.

We recognize a few additional simplifications in our model. First, our model ignored cell-cell transmission of infection. CD81 appears to be necessary for direct cell-cell transmission [47]. If the susceptibility of a cell to cell-cell transmission depends on CD81 expression in a manner similar to its susceptibility to viral entry, which remains to be ascertained, then we can show that our model with the pseudo-steady state approximation, $pI \approx cV$, implicitly accounts for cell-cell transmission: the net infection rate from both modes, $\beta_V S_i T_i V + \beta_I S_i T_i I \approx \beta_V S_i T_i V + \beta_I S_i T_i (cV/p) = \beta S_i T_i V$, is in agreement with our model (Eq. (1)) with β an effective infection rate constant that lumps the rate constants of infection by free virions, β_V, and cell-cell transmission, β_I. Second, our model assumes that reaction equilibrium is attained rapidly compared to viral entry and that the diffusion of CD81 on the target cells continually replenishes the free CD81 in the virus-cell contact region lost due to binding. Accordingly, our model predicts an upper bound on the mean number of E2-CD81 complexes formed in the contact region. Thus, if CD81 diffusion or its binding with E2 were rate limiting, a threshold smaller than 1–13 E2-CD81 complexes is expected to describe the data we considered. Finally, we ignored the splitting of cell culture at confluence. We employed the data at day 3 post-infection from Koutsoudakis et al. [13], when cells are not expected to have reached confluence. Further, the best-fit parameter estimates obtained from the data of Koutsoudakis et al. [13] were close to those from Zhong et al. [15] (Fig. 4). Also, accounting for splitting did not significantly alter our comparisons with the data of Tscherne et al. [14] so long as the splitting was performed after day 5 post-infection (Fig. S7). Also, including a logistic term to limit the proliferation of cells as they approached confluence did not alter our parameter estimates significantly (not shown). Nonetheless, that model predictions described several independent experimental observations quantitatively indicated that even with the above simplifications our model captured the essential features of HCV viral kinetics in vitro successfully. At the same time, the simplifications restricted model parameters to a number that allowed robust parameter estimation through fits to available data.

Methods

Model of HCV kinetics in vitro

We considered *in vitro* experiments where a population of uninfected cells, T, is exposed to a population of HCVcc virions, V. We divided the cells into K subpopulations, denoted T_i, where $i=1,2,..,K$, with cells in each subpopulation expressing CD81 in a range Δn_i around n_i molecules per unit area. At the start of infection ($t=0$), the variation of T_i with n_i was determined from a known distribution, $f(n_i)$, of CD81 expression levels across cells (Fig. 1). The following equations described the ensuing viral kinetics ($t>0$):

$$\frac{dT_i}{dt}=(\lambda-\mu)T_i-\beta S_i T_i V, \quad i=1,2,..,K \tag{1}$$

$$\frac{dI_i}{dt}=\beta S_i T_i V-\delta I_i, \quad i=1,2,..,K \tag{2}$$

$$\frac{dV}{dt}=p\sum_{i=1}^{K} I_i-cV \tag{3}$$

Here, λ and μ are the proliferation and death rates of T_i. β is the infection rate of cells expressing excess CD81. δ is the death rate of I_i. Following observations of HCV-induced cell cycle arrest in vitro [32,48], we neglected the proliferation of I_i. p and c are the per cell production rate and the clearance rate of free virions, respectively. Here, c represents the combined rate of the natural degradation of virions, the loss of viral infectivity, and the loss of virions due to entry and attachment [49,50]. For simplicity, we assumed c to be a constant.

To determine S_i, we considered a cell T_i, with CD81 expression level n_i, closely apposed to a virion with n_E E2 molecules per unit area. We assumed, as with HIV [20], that the E2-CD81 interactions across the virus-cell interface attain equilibrium well before viral entry. If B is the surface density of E2-CD81 complexes, C that of unbound CD81 and E that of unbound E2 molecules in the contact area, then at equilibrium $B=\frac{EC}{K_D^M}$, where K_D^M is the equilibrium dissociation constant of E2-CD81 complexes when the proteins are restricted to membranes. From Bell's analysis, $K_D^M=(4/3)RK_D$, where K_D is the equilibrium dissociation constant when the proteins are in solution and $R=0.75\,\mathrm{nm}$ is the encounter distance between the proteins for bond formation [51]. The virus-cell contact area, A, is small compared to the surface area of the cell. Further, free CD81 can diffuse on the cell membrane and therefore be recruited to the contact area. Consequently, C is expected not to decrease substantially below n_i, as suggested also by an independent reaction-diffusion model [52]. In contrast, the viral surface area is comparable to A and assuming E2 to be less mobile than CD81, it follows that the surface density of E2 in the contact area obeys the species balance equation: $E+B=n_E$. Under the latter two constraints, the mean number of complexes formed across the virus-cell contact at equilibrium, $\overline{N_C}$, is given by

$$\overline{N_C}=\frac{n_E n_i A}{K_D^M+n_i} \tag{4}$$

We recognized next that the E2 expression level on the virion and the virus-cell contact area are subject to stochastic variations. We assumed therefore that the number of complexes formed during a virus-cell contact, N_C, follows a Poisson distribution with mean $\overline{N_C}$. Viral entry (and subsequently infection) occurred if $N_C\geq N_C^T$, where N_C^T is the threshold number of E2-CD81 complexes necessary for HCV entry. The probability that $N_C\geq N_C^T$,

$$S_i=e^{-\overline{N_C}}\sum_{X=N_C^T}^{\infty}\frac{X^{\overline{N_C}}}{X!}, \tag{5}$$

thus yielded the relative susceptibility to infection of a cell with CD81 expression level n_i. (The Poisson distribution does allow N_C to exceed the limit of 180 set by the number of E2 molecules present on a virion, but in all our calculations $\overline{N_C}$ remained fewer than 30 (Fig. S8) so that the probability that $N_C\geq 180$ was negligibly small.)

Equations (1)–(5) yielded a model of HCV kinetics in vitro that accounted explicitly for the dependence of viral entry on the CD81 expression level on cells.

Model parameters and calculations

We solved model equations using a computer program written in MATLAB and computed quantities measured experimentally, namely, the time-evolution of the populations of uninfected and infected cells, $T=\sum_{i=1}^{K}T_i$ and $I=\sum_{i=1}^{K}I_i$, the viral titre, V, the fraction of cells infected, $\psi=\frac{I}{I+T}$, the fraction of cells infected within each subpopulation, $\xi_i=\frac{I_i}{I_i+T_i}$, $i=1,2,..,K$, and the populations of viable and dead cells, $T_v=T+I$ and $T_d=\int_0^t(\mu T(s)+\delta I(s))ds$, respectively.

We employed the following parameter values and initial conditions: $n_E=2.3\times10^4\,\mu\mathrm{m}^{-2}$ corresponding to 180 E2 molecules on a virion with average diameter 50 nm [53]; $A=1.3\times10^{-3}\,\mu\mathrm{m}^2$, corresponding to a virus-cell contact radius of 20 nm [54]; the target cell diameter was $60\,\mu\mathrm{m}$ [17]; K_D was varied over the range $\sim10^{-5}-10^{-4}\,\mathrm{M}$ (see above). The initial CD81 expression was assumed to follow the log-normal distribution, $f(n_i)=\frac{1}{n_i\sigma\sqrt{2\pi}}e^{-\frac{(\ln n_i-v)^2}{2\sigma^2}}$, where v and σ were the mean and standard deviation of $\ln n_i$. For comparisons with experimental data, the initial distributions were obtained from measurements (Fig. S2; see below). Thus, the initial cell subpopulations, $T_i(0)=f(n_i)\Delta n_i T(0)$, where $T(0)$ was the total initial target cell population. We divided the range of CD81 expression levels into $K=80$ intervals, which determined Δn_i; finer discretisation did not improve the accuracy of our solution (Fig. S1). The remaining parameters, estimated from fits to data, are listed in Tables S1 and S2. We have summarized model parameters in Table 1.

Data and fitting

We considered data from three recently published cell culture studies of HCV kinetics. First, we considered data of Zhong et al. [15], where Huh-7.5.1 cells were exposed to JFH-1 virions and the kinetics of infection followed for 21 d. Specifically, we employed the data of the time-evolution of the supernatant infectivity, the population of attached (viable) cells, and the ratio of the populations of floating (dead) and attached cells, the latter two datasets with mock infection as well as with HCVcc infection (Fig. S1 in [15]). Second, we considered data of Koutsoudakis et al. [13], where a 1:1 mixture of Huh7-Lunet and Lunet/CD81 cells was exposed to HCVcc Venus-Jc1 virus and the fractions of cells

infected in subpopulations with distinct CD81 expression levels were measured after 72 h. The initial viral population was at an MOI of ~5 and ~1 $TCID_{50}$/cell (where $TCID_{50}$ is the 50% tissue culture infective dose), respectively, in two independent experiments (Fig. 5 in [13]). Third, we considered the data of Tscherne et al. [14], where Huh7.5 cells were exposed to J6/JFH virus and the time-evolution of the fraction of cells infected as well as of the distribution of CD81 expression levels across cells was followed for 17 d (Fig. 8 in [14]).

The CD81 expression on cells is usually measured in terms of fluorescent intensity. To convert the measurements to CD81 surface densities, we adopted the following procedure. Measured distributions of the CD81 expression level on Huh-7.5 (silRR) cells were digitized from Zhang et al. [55] and on Huh-7.5 cells from Koutsoudakis et al. [13]. The log-normal distribution, $y=\frac{A}{x}e^{-\frac{(\ln x-v)^2}{2\sigma^2}}$, yielded good fits to the data (Fig. S9). The best-fit parameter values (95% CI) were $v_Z=4.29$ (4.27–4.31) and $\sigma_Z=0.45$ (0.43–0.47) for the data of Zhang et al. and $v_K=6.1$ (6.07–6.12) and $\sigma_K=0.7$ (0.67–0.72) for the data of Koutsoudakis et al. Because the same cell lines were used, the underlying distributions of CD81 expression are expected to be similar in the two experiments. The differences in the reported fluorescence intensities may therefore be attributed to different conversions of CD81 surface density to fluorescence intensity in the two measurements. To unravel the underlying distribution, we assumed that log fluorescence intensity was linearly proportional to log CD81 surface density (or that the fluorescence intensity had a power law dependence on the surface density). Thus, a cell with CD81 surface density n_i would yield a fluorescence intensity z_i and k_i in the measurements of Zhang et al. and Koutsoudakis et al., respectively, such that $\ln n_i=a+b\ln z_i$ and $\ln n_i=c+d\ln k_i$, where a, b, c, and d are constants. To determine the latter constants, we employed the following observations: The mean surface density of CD81 for the Huh-7 cell line is 2×10^5 molecules/cell [3], which corresponded to a fluorescence intensity of 48 units in the measurements of Zhang et al., so that $\ln 2\times10^5=a+b\ln 48$. Also, Koutsoudakis et al. measured the number of CD81 molecules/cell corresponding to a fluorescence intensity of 100 units and found it to be 7×10^4 molecules/cell, so that $\ln 7\times10^4=c+d\ln 100$. Further the above relationship between fluorescence intensity and CD81 expression also implied that $a+b\ln v_z=c+d\ln v_k$ and $b\sigma_Z=d\sigma_K$. Solving the latter equations using the best-fit parameters above, we obtained $a=2.8$, $b=2.43$, $c=3.96$ and $d=1.56$, which enabled conversion of measured fluorescence intensities to CD81 surface densities, n_i (Fig. S2). The measured distributions in terms of counts versus fluorescence intensities were then converted to probability distributions, $f(n_i)$ versus n_i, by normalizing the counts such that the areas under the $f(n_i)$ versus n_i curves equalled unity. The resulting distributions (Fig. S2) were employed as the initial CD81 distributions for our fits to data (Fig. 3).

We digitized data using Engauge digitizer and fit model predictions to data using the nonlinear regression tool NLINFIT in MATLAB.

Supporting Information

Figure S1 Sensitivity to model parameters. Time-evolution of (A) uninfected cells, T, (B) infected cells, I, (C) viral load, V, and (D) the fraction of cells infected, ψ, obtained by varying (I) the equilibrium dissociation constant, $K_D=1.7\times10^{-5}$ M (thick solid line), 3.3×10^{-5} M (thin solid line), and 1.7×10^{-4} M (dashed line), (II) the mean of the log initial CD81 expression level, $v=29.8$ (thick solid line), 31.8 (thin solid line), and 33.8 (dashed line), (III) the initial viral load, $V_0=40$ ffu·ml^{-1} (thick solid line), 400 ffu·ml^{-1} (thin solid line), and 4000 ffu·ml^{-1} (dashed line), (IV) the infection rate constant, $\beta=1.2\times10^{-3}$ ml·(ffu·d)$^{-1}$ (thick solid line), 1.2×10^{-4} ml·(ffu·d)$^{-1}$ (thin solid line), and 1.2×10^{-5} ml·(ffu·d)$^{-1}$ (dashed line), (V) the viral production rate, $p=0.278$ ffu·(ml·d)$^{-1}$ (thick solid line), 2.78 ffu·(ml·d)$^{-1}$ (thin solid line), and 27.8 ffu·(ml·d)$^{-1}$ (dashed line), and (VI) the number of cell sub-populations, $K=40$ (thick solid line), 80 (thin solid line), and 120 (dashed line). (The three curves in (VI) are indistinguishable.)
(TIF)

Figure S2 Initial distribution of the CD81 expression level on target cells. Distribution of the CD81 expression level on (A) Huh-7.5 cells and (B) Huh7-Lunet cells (diamonds) and Lunet/CD81 cells (circles) obtained by digitizing data from Koutsoudakis et al. (2007) J Virol 81:588–598 and converting fluorescence intensities to CD81 surface densities (Methods).
(TIF)

Figure S3 Approximating the Poisson distribution with a truncated Gaussian distribution. Model predictions of the susceptibility of cells using the Poisson distribution, $S_i=e^{-\overline{N_C}}\sum_{X=N_C^T}^{\infty}\frac{X^{\overline{N_C}}}{X!}$ (dashed line), and an equivalent truncated Gaussian distribution with mean $\overline{N_C}$ and standard deviation $\sqrt{\overline{N_C}}$, which yields $S_i=\frac{\mathrm{erfc}\left(\frac{\left(N_C^T-0.5\right)-\overline{N_C}}{\sqrt{2\overline{N_C}}}\right)}{\mathrm{erfc}\left(-\sqrt{\frac{\overline{N_C}}{2}}\right)}$ (solid line), where $\mathrm{erfc}(z)=\frac{2}{\sqrt{\pi}}\int_z^{\infty}\exp(-t^2)dt$ is the complementary error function, for different values of N_C^T and for (A) $K_D=1.7\times10^{-5}$ M and (B) $K_D=3.3\times10^{-4}$ M.
(TIF)

Figure S4 Comparisons of model predictions with data using different values of K_D. (A) The fit in Fig. 3B repeated with $K_D=1.7\times10^{-5}$ M (thick solid line), 3.3×10^{-5} M (thin solid line), 1.7×10^{-4} M (dashed line), and 3.3×10^{-4} M (dotted line). The resulting best-fit parameter estimates are in Table S1. (The fits for different K_D nearly overlap and are indistinguishable.) (B) Fits in Fig. 3C repeated with the above values of K_D. The resulting best-fit parameter estimates are in Table S2. (C) The comparison in Fig. 3D repeated with the above values of K_D and other parameter values in Table S1.
(TIF)

Figure S5 Fits without the pseudo-steady state approximation. The pseudo-steady state approximation is relaxed and our model predictions (Eqs. (1)–(5)) are fit to the data in Fig. 3B using the parameter estimates in Table S1 and with viral clearance rate c as an adjustable parameter. Initial conditions used are: $T(0)=3.7\times10^4$ cells; $V(0)=400$ ffu·ml^{-1}; $T_d(0)=I(0)=0$. The resulting estimates of c are 21.4, 22.7, 23.2 and 23.8 d^{-1} for $K_D=1.7\times10^{-5}$, 3.3×10^{-5}, 1.7×10^{-4}, and 3.3×10^{-4} M, respectively. (The fits for different K_D nearly overlap and are indistinguishable.)
(TIF)

Figure S6 Susceptibility of cells predicted using different best-fit parameter combinations. Dependence of S_i on CD81 expression predicted using the parameter combinations in (A) Table S1 and (B) Table S2 where $K_D=1.7\times10^{-5}$ M (thick solid line), 3.3×10^{-5} M (thin solid line), 1.7×10^{-4} M (dashed line), and 3.3×10^{-4} M (dotted line).
(TIF)

Figure S7 Influence of splitting of cell culture at confluence. Model predictions of the fraction of cells infected without splitting (thick line), splitting at day 6 and day 12 (thin line), and splitting at day 8 and day 12 (dashed line) after the onset of infection compared with the data in Fig. 3D (symbols). Parameters used are the same as in Fig. 3D.
(TIF)

Figure S8 Mean number and probability of formation of E2-CD81 complexes. (A) Model predictions of the mean number of E2-CD81 complexes formed, $\overline{N_C}$, as a function of CD81 expression for $K_D = 1.7\times10^{-5}$ M (solid line), 3.3×10^{-5} M (dashed line), 1.7×10^{-4} M (dashed-dotted line), and 3.3×10^{-4} M (dotted line). (B) Model predictions of the Poisson probability of forming N_C E2-CD81 complexes (Eq. (5)) when $\overline{N_C}=1$ (solid line) and $\overline{N_C}=30$ (dashed line).
(TIF)

Figure S9 Conversion of fluorescence intensity to CD81 expression. Measured distributions of the CD81 expression level on Huh-7.5 (silRR) cells digitized from Zhang et al. (2004) J Virol 78:1448–1445 (diamonds) and Huh-7.5 cells from Koutsoudakis et al. (2007) J Virol 81:588–598 (triangles). Lines are best-fits of the log-normal distribution, $y=\frac{A}{x}e^{-\frac{(\ln x-v)^2}{2\sigma^2}}$, to the data. The best-fit parameter values (95% CI) are $v_Z = 4.29$ (4.27–4.31) and $\sigma_Z = 0.45$ (0.43–0.47) for the data of Zhang et al. and $v_K = 6.1$ (6.07–6.12) and $\sigma_K = 0.7$ (0.67–0.72) for the data of Koutsoudakis et al.
(TIF)

Table S1 Estimates of model parameters obtained from fits of model predictions to the data in Figs. 3B and S4A. 95% confidence intervals are indicated in brackets.
(DOC)

Table S2 Estimates of model parameters obtained from fits of model predictions to the data in Figs. 3C and S4B. 95% confidence intervals are indicated in brackets.
(DOC)

Acknowledgments

We are grateful to Donna Tscherne, Thomas Pietschmann and Jin Zhong for discussions and for providing details of their experiments.

Author Contributions

Conceived and designed the experiments: PP NMD. Performed the experiments: PP. Analyzed the data: PP NMD. Contributed reagents/materials/analysis tools: PP NMD. Wrote the paper: PP NMD.

References

1. Scarselli E, Ansuini H, Cerino R, Roccasecca RM, Acali S, et al. (2002) The human scavenger receptor class B type I is a novel candidate receptor for the hepatitis C virus. EMBO J 21: 5017–5025.
2. Pileri P, Uematsu Y, Campagnoli S, Galli G, Falugi F, et al. (1998) Binding of hepatitis C virus to CD81. Science 282: 938–941.
3. Cormier EG, Tsamis F, Kajumo F, Durso RJ, Gardner JP, et al. (2004) CD81 is an entry coreceptor for hepatitis C virus. Proc Natl Acad Sci U S A 101: 7270–7274.
4. Evans MJ, von Hahn T, Tscherne DM, Syder AJ, Panis M, et al. (2007) Claudin-1 is a hepatitis C virus co-receptor required for a late step in entry. Nature 446: 801–805.
5. Ploss A, Evans MJ, Gaysinskaya VA, Panis M, You H, et al. (2009) Human occludin is a hepatitis C virus entry factor required for infection of mouse cells. Nature 457: 882–886.
6. Law M, Maruyama T, Lewis J, Giang E, Tarr AW, et al. (2008) Broadly neutralizing antibodies protect against hepatitis C virus quasispecies challenge. Nat Med 14: 25–27.
7. Dorner M, Horwitz JA, Robbins JB, Barry WT, Feng Q, et al. (2011) A genetically humanized mouse model for hepatitis C virus infection. Nature 474: 208–211.
8. Fafi-Kremer S, Fofana I, Soulier E, Carolla P, Meuleman P, et al. (2010) Viral entry and escape from antibody-mediated neutralization influence hepatitis C virus reinfection in liver transplantation. J Exp Med 207: 2019–2031.
9. Krieger SE, Zeisel MB, Davis C, Thumann C, Harris HJ, et al. (2009) Inhibition of hepatitis C virus infection by anti-claudin-1 antibodies is mediated by neutralization of E2-CD81-claudin-1 associations. Hepatology 51: 1144–1157.
10. Harris HJ, Davis C, Mullins JGL, Hu K, Goodall M, et al. (2010) Claudin association with CD81 defines hepatitis C virus entry. J Biol Chem 285: 21092–21102.
11. Lemon SM, McKeating JA, Pietschmann T, Frick DN, Glenn JS, et al. (2010) Development of novel therapies for hepatitis C. Antivir Res 86: 79–92.
12. Zeisel MB, Fofana I, Fafi-Kremer S, Baumert TF (2011) Hepatitis C virus entry into hepatocytes: Molecular mechanisms and targets for antiviral therapies. J Hepatol 54: 566–576.
13. Koutsoudakis G, Herrmann E, Kallis S, Bartenschlager R, Pietschmann T (2007) The level of CD81 cell surface expression is a key determinant for productive entry of hepatitis C virus into host cells. J Virol 81: 588–598.
14. Tscherne DM, Evans MJ, von Hahn T, Jones CT, Stamataki Z, et al. (2007) Superinfection exclusion in cells infected with hepatitis C virus. J Virol 81: 3693–3703.
15. Zhong J, Gastaminza P, Chung J, Stamataki Z, Isogawa M, et al. (2006) Persistent hepatitis C virus infection in vitro: coevolution of virus and host. J Virol 80: 11082–11093.
16. Kapadia SB, Barth H, Baumert T, McKeating JA, Chisari FV (2007) Initiation of hepatitis C virus infection is dependent on cholesterol and cooperativity between CD81 and scavenger receptor B type I. J Virol 81: 374–383.
17. Brazzoli M, Bianchi A, Filippini S, Weiner A, Zhu Q, et al. (2008) CD81 is a central regulator of cellular events required for hepatitis C virus infection of human hepatocytes. J Virol 82: 8316–8329.
18. Zhang YY, Zhang BH, Ishii K, Liang TJ (2010) Novel function of CD81 in controlling hepatitis C virus replication. J Virol 84: 3396–3407.
19. Magnus C, Rusert P, Bonhoeffer S, Trkola A, Regoes RR (2009) Estimating the stoichiometry of human immunodeficiency virus entry. J Virol 83: 1523–1531.
20. Mulampaka SN, Dixit NM (2011) Estimating the threshold surface density of gp120-CCR5 complexes necessary for HIV-1 envelope-mediated cell-cell fusion. PLoS One 6: e19941.
21. Neumann AU, Lam NP, Dahari H, Gretch DR, Wiley TE, et al. (1998) Hepatitis C viral dynamics in vivo and the antiviral efficacy of interferon-alpha therapy. Science 282: 103–107.
22. Zeuzem S, Herrmann E, Lee JH, Fricke J, Neumann AU, et al. (2001) Viral kinetics in patients with chronic hepatitis C treated with standard or peginterferon alpha-2a. Gastroenterology 120: 1438–1447.
23. Herrmann E, Lee JH, Marinos G, Modi M, Zeuzem S (2003) Effect of ribavirin on hepatitis C viral kinetics in patients treated with pegylated interferon. Hepatology 37: 1351–1358.
24. Dixit NM, Layden-Almer JE, Layden TJ, Perelson AS (2004) Modelling how ribavirin improves interferon response rates in hepatitis C virus infection. Nature 432: 922–924.
25. Dahari H, Ribeiro RM, Perelson AS (2007) Triphasic decline of hepatitis C virus RNA during antiviral therapy. Hepatology 46: 16–21.
26. Colombatto P, Ciccorossi P, Maina AM, Civitano L, Oliveri F, et al. (2008) Early and accurate prediction of peg-IFNs/ribavirin therapy outcome in the individual patient with chronic hepatitis C by modeling the dynamics of the infected cells. Clin Pharmacol Ther 84: 212–215.
27. Rong L, Dahari H, Ribeiro RM, Perelson AS (2010) Rapid emergence of protease inhibitor resistance in hepatitis C virus. Sci Transl Med 2: 30ra32.
28. Rong L, Perelson AS (2010) Treatment of hepatitis C virus infection with interferon and small molecule direct antivirals: viral kinetics and modeling. Crit Rev Immunol 30: 131–148.
29. Adiwijaya BS, Herrmann E, Hare B, Kieffer T, Lin C, et al. (2010) A multi-variant, viral dynamic model of genotype 1 HCV to assess the in vivo evolution of protease-inhibitor resistant variants. PLoS Comput Biol 6: e1000745.
30. Guedj J, Perelson AS (2011) Second-phase hepatitis C virus RNA decline during telaprevir-based therapy increases with drug effectiveness: Implications for treatment duration. Hepatology 53: 1801–1808.
31. Hsu CS, Hsu SJ, Chen HC, Tseng TC, Liu CH, et al. (2011) Association of IL28B gene variations with mathematical modeling of viral kinetics in chronic hepatitis C patients with IFN plus ribavirin therapy. Proc Natl Acad Sci U S A 108: 3719–3724.
32. Walters KA, Syder AJ, Lederer SL, Diamond DL, Paeper B, et al. (2009) Genomic analysis reveals a potential role for cell cycle perturbation in HCV-mediated apoptosis of cultured hepatocytes. PLoS Pathog 5: e1000269.
33. DebRoy S, Kribs-Zaleta C, Mubayi A, Cardona-Melendez GM, Medina-Rios L, et al. (2010) Evaluating treatment of hepatitis C for hemolytic anemia management. Mathematical Biosciences 225: 141–155.
34. Krishnan SM, Dixit NM (2011) Ribavirin-induced anemia in hepatitis C virus patients undergoing combination therapy. PLoS Comput Biol 7: e1001072.

35. Wakita T, Pietschmann T, Kato T, Date T, Miyamoto M, et al. (2005) Production of infectious hepatitis C virus in tissue culture from a cloned viral genome. Nat Med 11: 791–796.
36. Zhong J, Gastaminza P, Cheng G, Kapadia S, Kato T, et al. (2005) Robust hepatitis C virus infection in vitro. Proc Natl Acad Sci U S A 102: 9294–9299.
37. Lindenbach BD, Evans MJ, Syder AJ, Wölk B, Tellinghuisen TL, et al. (2005) Complete replication of hepatitis C virus in cell culture. Science 309: 623–626.
38. Ploss A, Khetani SR, Jones CT, Syder AJ, Trehan K, et al. (2010) Persistent hepatitis C virus infection in microscale primary human hepatocyte cultures. Proc Natl Acad Sci U S A 107: 3141–3145.
39. Guedj J, Neumann AU (2010) Understanding hepatitis C viral dynamics with direct-acting antiviral agents due to the interplay between intracellular replication and cellular infection dynamics. J Theor Biol 267: 330–340.
40. Dahari H, Ribeiro RM, Rice CM, Perelson AS (2007) Mathematical modeling of subgenomic hepatitis C virus replication in Huh-7 cells. J Virol 81: 750–760.
41. Dahari H, Sainz B, Jr., Perelson AS, Uprichard SL (2009) Modeling subgenomic hepatitis C virus RNA kinetics during treatment with alpha interferon. J Virol 83: 6383–6390.
42. Hofmann WP, Zeuzem S (2011) A new standard of care for the treatment of chronic HCV infection. Nat Rev Gastroenterol Hepatol 8: 257–264.
43. Nakajima H, Cocquerel L, Kiyokawa N, Fujimoto J, Levy S (2005) Kinetics of HCV envelope proteins' interaction with CD81 large extracellular loop. Biochem Biophys Res Commun 328: 1091–1100.
44. Baksh MM, Kussrow AK, Mileni M, Finn MG, Bornhop DJ (2011) Label-free quantification of membrane-ligand interactions using backscattering interferometry. Nat Biotechnol 29: 357–360.
45. Flint M, Von Hahn T, Zhang J, Farquhar M, Jones CT, et al. (2006) Diverse CD81 proteins support hepatitis C virus infection. J Virol 80: 11331–11342.
46. Rocha-Perugini V, Lavie M, Delgrange D, Canton J, Pillez A, et al. (2009) The association of CD81 with tetraspanin-enriched microdomains is not essential for hepatitis C virus entry. BMC Microbiol 9: 111.
47. Brimacombe CL, Grove J, Meredith LW, Hu K, Syder AJ, et al. (2011) Neutralizing antibody resistant hepatitis C virus cell-to-cell transmission. J Virol 85: 596–605.
48. Kannan RP, Hensley LL, Evers LE, Lemon SM, McGivern DR (2011) Hepatitis C virus infection causes cell cycle arrest at the level of initiation of mitosis. J Virol 85: 7989–8001.
49. Beauchemin CAA, McSharry JJ, Drusano GL, Nguyen JT, Went GT, et al. (2008) Modeling amantadine treatment of influenza A virus in vitro. J Theor Biol 254: 439–451.
50. Sabahi A, Marsh KA, Dahari H, Corcoran P, Lamora JM, et al. (2010) The rate of hepatitis C virus infection initiation in vitro is directly related to particle density. Virology 407: 110–119.
51. Bell GI (1978) Models for the specific adhesion of cells to cells. Science 200: 618–627.
52. Wu J, Fang Y, Zarnitsyna VI, Tolentino TP, Dustin ML, et al. (2008) A coupled diffusion-kinetics model for analysis of contact-area FRAP experiment. Biophys J 95: 910–919.
53. Yu X, Qiao M, Atanasov I, Hu Z, Kato T, et al. (2007) Cryo-electron microscopy and three-dimensional reconstructions of hepatitis C virus particles. Virology 367: 126–134.
54. Sougrat R, Bartesaghi A, Lifson JD, Bennett AE, Bess JW, et al. (2007) Electron tomography of the contact between T cells and SIV/HIV-1: implications for viral entry. PLoS Pathog 3: e63.
55. Zhang J, Randall G, Higginbottom A, Monk P, Rice CM, et al. (2004) CD81 is required for hepatitis C virus glycoprotein-mediated viral infection. J Virol 78: 1448–1455.